Research Article | Vol. 30, No. 14 / 4 Jul 2022 / Optics Express 25308
Optics EXPRESS

Compact 100GBaud driverless thin-film lithium niobate modulator on a silicon substrate

GENGXIN CHEN,[1] KAIXUAN CHEN,[2,3] JUNWEI ZHANG,[4,5] RANFENG GAN,[2] LU QI,[2] XUANCONG FAN,[2,3] ZILIANG RUAN,[1] ZHENRUI LIN,[4] JIE LIU,[4] CHAO LU,[5] ALAN PAK TAO LAU,[6] DAOXIN DAI,[1,7] CHANGJIAN GUO,[2,3,8] AND LIU LIU[1,9]

[1]*State Key Laboratory for Modern Optical Instrumentation, College of Optical Science and Engineering, International Research Center for Advanced Photonics, Zhejiang University, Hangzhou 310058, China*
[2]*Guangdong Provincial Key Laboratory of Optical Information Materials and Technology, South China Academy of Advanced Optoelectronics, Sci, Bldg. No.5, South China Normal University, Higher-Education Mega-Center, Guangzhou 510006, China*
[3]*National Center for International Research on Green Optoelectronics, South China Normal University, Guangzhou 510006, China*
[4]*State Key Laboratory of Optoelectronic Materials and Technologies, School of Electronics and Information Technology, Sun Yat-Sen University, Guangzhou 510006, China*
[5]*Photonics Research Center, Department of Electronic and Information Engineering, The Hong Kong Polytechnic University, Hong Kong SAR, China*
[6]*Photonics Research Center, Department of Electrical Engineering, The Hong Kong Polytechnic University, Hong Kong SAR, China*
[7]*Jiaxing Key Laboratory of Photonic Sensing & Intelligent Imaging, Intelligent Optics & Photonics Research Center, Jiaxing Research Institute Zhejiang University, Jiaxing 314000, China*
[8]*changjian.guo@coer-scnu.org*
[9]*liuliuopt@zju.edu.cn*

Abstract: Electro-optic (EO) modulators with a high modulation bandwidth are indispensable parts of an optical interconnect system. A key requirement for an energy-efficient EO modulator is the low drive voltage, which can be provided using a standard complementary metal oxide semiconductor circuity without an amplifying driver. Thin-film lithium niobate has emerged as a new promising platform, and shown its capable of achieving driverless and high-speed EO modulators. In this paper, we report a compact high-performance modulator based on the thin-film lithium niobate platform on a silicon substrate. The periodic capacitively loaded travelling-wave electrode is employed to achieve a large modulation bandwidth and a low drive voltage, which can support a driverless single-lane 100Gbaud operation. The folded modulation section design also helps to reduce the device length by almost two thirds. The fabricated device represents a large EO bandwidth of 45GHz with a half-wave voltage of 0.7V. The driverless transmission of a 100Gbaud 4-level pulse amplitude modulation signal is demonstrated with a power consumption of 4.49fj/bit and a bit-error rate below the KP4 forward-error correction threshold of 2.4×10^{-4}.

1. Introduction

The fast developments of high-definition streaming media, 5G, cloud-based service, artificial intelligence, and internet of things result in an explosive traffic growth in data communications, which leads to a dramatic increase in demand for energy. It is predicted that datacenters will account for 20% of worldwide electricity consumption [1]. Optical interconnect is a promising option to overcome transmission bottlenecks in datacenters and high-performance computers [2]. An electro-optic (EO) modulator with a large bandwidth is one of the most important devices

#458431 https://doi.org/10.1364/OE.458431
Journal © 2022 Received 15 Mar 2022; revised 4 May 2022; accepted 15 Jun 2022; published 28 Jun 2022

Optics EXPRESS

in optical interconnect, which is needed to provide a fast data conversion from electrical to optical domain to ensure a high-speed data transmission [3]. In the past decades, EO modulators on different platforms have been intensively studied, such as silicon based modulators [4], silicon-organic-hybrid (SOH) modulators [5], plasmonic-organic hybrid modulators [6], indium phosphate (InP) modulators [7], and so on. A key requirement for energy-efficient EO modulators is a low drive voltage that can be provided by, e.g., a standard CMOS (complementary metal oxide semiconductor) circuitry without further amplification. Applying resonant structures such as microrings, silicon based modulators, relying on free-carrier dispersion in a pn junction, can achieve an ultra-low energy consumption of 5.3fj/bit operated at 128Gb/s on-off keying (OOK) modulation with an electrical drive signal of 0.8Vpp (peak-to-peak voltage) [8]. However, their performances are sensitive to the shift in the resonance wavelength due to fabrication imperfection or thermal effect. Although such shifts can be corrected with on-chip temperature controller, it is at the expense of an increased complexity and energy consumption. SOH modulators, benefiting from ultra-high Pockels coefficients of some engineered organic materials, can achieve much higher modulation efficiency than silicon based modulators. It has been demonstrated that SOH modulators can support sub-fj/bit power consumption [9]. However, the data transmission is still limited at 40Gb/s for a simple OOK modulation [9,10], and the thermal stability of organic materials still needs to be validated [11]. Thin-film lithium niobate (TFLN) modulators emerged recently as a new candidate for the next generation of high-speed optical interconnect devices. The TFLN based modulators offer a significant improved voltage-bandwidth performance compared with traditional titanium-diffused LN modulators without scarifying any key material properties [12]. However, due to an intrinsic trade-off in the voltage-bandwidth performance of a travelling-wave (TW) Mach-Zehnder interferometer (MZI) modulator, driverless TFLN modulators based on the regular electrode structure only support OOK modulation up to 70Gb/s so far [12]. Recently, the periodic capacitively-loaded travelling-wave (CLTW) electrode structure is proposed on TFLN platform on quartz [13,14] and silicon [15] substrates to break this compromise. Therefore, TFLN modulators with both a high bandwidth and a low drive voltage can be realized [13–15]. On the other hand, due to the moderate Pockels coefficient of the LN material, such a sub-one-volt TFLN modulator normally requires a several-centimeter long modulation section, which also limits their applications when the chip length is restricted. Folded modulator structure has been, therefore, proposed to shorten the physical length of a TFLN modulator, at a cost of its width, by using either poling process [16] or waveguide crossings [17].

In this paper, we demonstrate a folded MZI (FMZI) modulator on the TFLN platform using a CLTW electrode. The silicon undercut etching technique is introduced to achieve the necessary velocity matching between the optical and radio frequency (RF) waves. Waveguide U-turns and TW electrode U-turns are introduced to fold the modulation section twice. The proposed FMZI modulator shows outstanding voltage-bandwidth performance of an EO bandwidth BW_{3dB} of about 45 GHz with <0.7 V halfwave-voltage V_π. This level of drive signal can be achieved without using a RF amplifier [18], which helps reduce the power consumption of the data transmitter. 4-level pulse amplitude (PAM-4) modulation up to 100GBaud are successfully demonstrated with a power consumption of <5fj/bit.

2. Device design and fabrication

A three-dimensional (3D) view of the proposed FMZI modulator on the TFLN platform using the CLTW electrode is shown in Fig. 1. The device is fabricated on a commercial x-cut LN-on-insulator wafer (NanoLN) with a 725μm thick silicon substrate layer, a 3μm thick buried oxide (BOX) layer, and a 400 nm thick TFLN layer. The TFLN waveguide has a ridge height of 200 nm, (i.e., half of the TFLN total thickness), and its width at the modulation section is 1.5μm. Grating couplers (GCs) are used as fiber-to-chip interfaces [19,20]. Multimode interferometers (MMIs) made also on TFLN are used as the 3 dB beam splitter and combiner for the MZI

Optics EXPRESS

structure. To reduce the length of the modulator chip, FMZI structure with two U-turns are adopted here. In order to maintain a consistent direction of the applied electric field in each MZI arm, a waveguide crossing is applied at each U-turn [17], as shown in Figs. 1(a) and 1(d). The bending radius of the TFLN waveguide is 150μm to ensure a low-loss transmission of the fundamental transverse-electrical (TE) mode without stimulating any higher-order modes [21]. The parameters of the TFLN waveguide crossing are optimized, which gives (w_1, w_2, l_1, l_2) (0.72, 3.58, 10, 29.2) μm. Theoretically, a negligible insertion loss and a crosstalk of −36 dB can be obtained. The whole TFLN structure is coated with a 900nm-thick SiO_2 over-cladding layer, on top of which, the CLTW electrode based on a coplanar-line RF waveguide with periodically loaded T-segments is adopted. Compared with traditional TW electrode designs with higher RF losses [13] (and hence a poor high-frequency modulation performance), here the width of the unloaded signal electrode W_s is 75μm, which is designed large enough to decrease conductor losses for the RF waves. The width of unloaded ground electrode W_g is set to 200μm, which should ensure a low crosstalk between adjacent RF waveguides. The rest parameters of the CLTW electrode are carefully design to satisfy both impedance and index matching, which gives (*g*, *r*, *c*, *s*, *t*, *h*, *hw*, *hl*, *tl*, *tu*, *hr*) (1.8, 47, 3, 2, 5, 15, 9, 39, 0.9, 1.1, 35) μm [15]. The above electrode parameters correspond to a radius of the RF waveguide U-turn of 173.6μm, measured from the center of the signal electrode. The U-turn sections are designed using an ordinary coplanar-line waveguide without the T-segments.

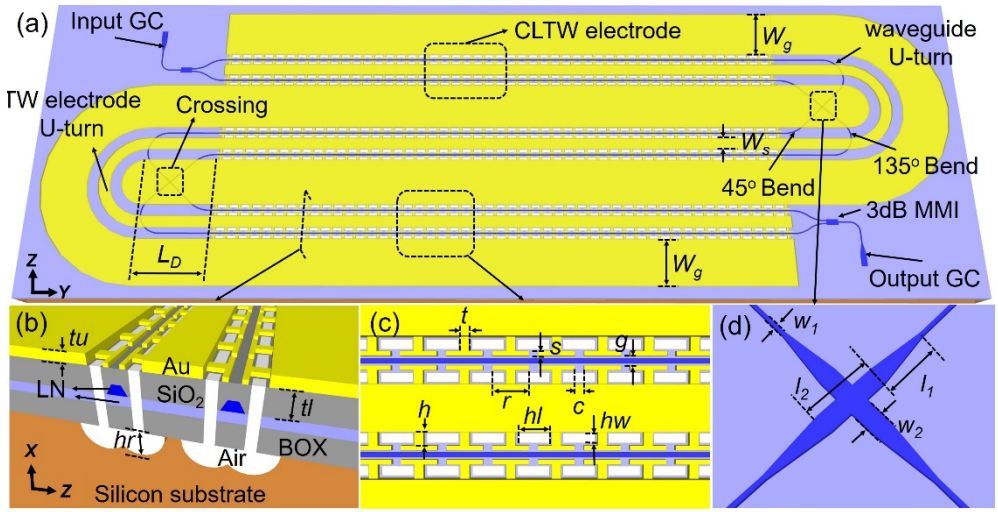

Fig. 1. Proposed FMZI modulator on the TFLN platform using the CLTW electrode. 3D view of (a) whole structure and (b) cross-sectional structure of the modulation section. Top view of (c) CLTW electrode and (d) crossing TFLN waveguide at the U-turn.

We simulated the electrical and optical modes of the proposed structure using a finite element algorithm (COMSOL). The modulation efficiency $V_\pi L = 2.10$V·cm can be derived with a low optical propagation loss of ~0.04 dB/cm theoretically for the fundamental TE mode. It is known that the walk-off between the optical and RF waves can dramatically reduce the EO bandwidth BW_{3dB}. Since a perfect index matching between them is designed for the straight modulation sections, the optical and RF time delays through the U-turns have also to be matched to ensure a wide bandwidth. As the fundamental TE mode group index of the TFLN waveguide is 2.20, the total optical time delay through one U-turn in the present design is $\Delta\sigma_{opt} = \Delta\sigma_{straight} + \Delta\sigma_{bend} + \Delta\sigma_{cross} = 6.24$ps. The RF effective index at the U-turn section (no T-segments) is $n_m = 2.33$, the RF time delay through a 180° circular bending is $\Delta\sigma_{RF} = 4.27$ps, which is less than $\Delta\sigma_{opt}$.

Optics EXPRESS

Therefore, as shown in Fig. 1(a), an additional delay length of L_D needs to be introduced for the RF waveguide at the U-turn, which can be calculated as $L_D = \frac{(6.24-4.27)\times c}{2\times n_m} = 127\mu$m, where c is speed of light in free space.

The fabrication processes of the designed FMZI modulator include TFLN structures patterning, SiO_2 over-cladding deposition, metal electrode deposition, and undercut hole etching, which has been discussed in Ref. [15] in details. Figures 2(a)–2(d) show some images of the fabricated devices. For comparison, a straight MZI (SMZI) modulator using the same CLTW electrode without folding was also fabricated on the same wafer. Thanks to the folded structure, the length of the FMZI modulator is reduced to 38% of that of the SMZI modulator.

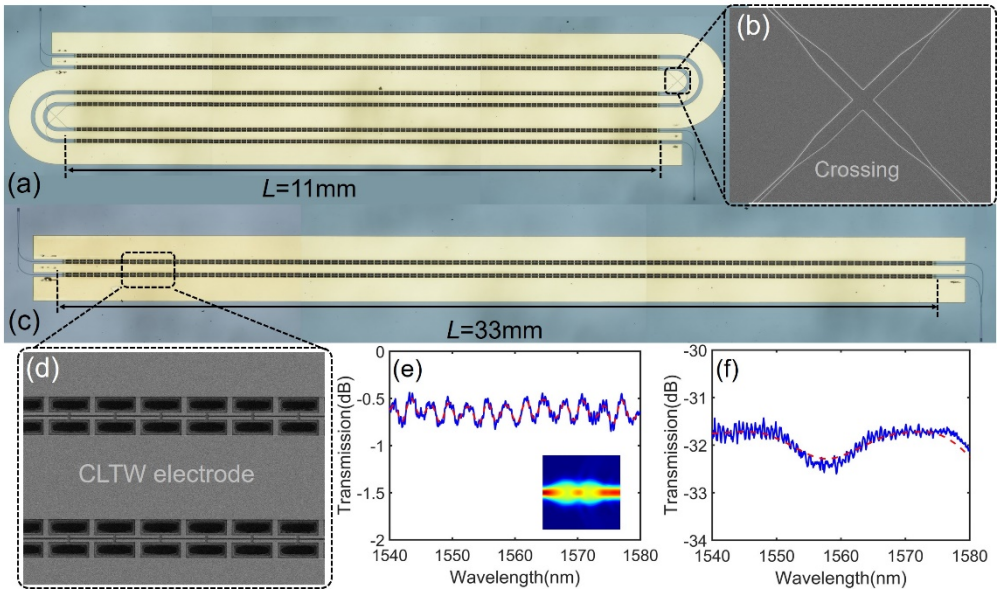

Fig. 2. Scanning electron microscopy images of (a) FMZI modulator, (b) TFLN waveguide crossing at the U-turn, (c) SMZI modulator with the same modulation length for reference, and (d) CLTW electrode. (e) Measured optical insertion losses of 8 cascaded crossings. Inset shows the simulated light propagation in the crossing. (f) Measured crosstalk spectrum of the crossing.

3. Measurement and analysis

First, the TFLN waveguide crossing was characterized with a sperate testing structure. The measured losses of 8 cascaded crossings are about −0.72 dB, as shown in Fig. 2(e), which corresponds to an insertion loss of −0.09 dB for a single crossing. The measured crosstalk is well below −31 dB, as shown in Fig. 2(f). The fabricated SMZI and FMZI modulators with modulation section length of 33 mm were then characterized as shown in Fig. 3. The total optical loss of the chip is about 14 dB, with on-chip insertion losses of 5.8 ± 0.2 dB for both types of modulators. The static extinction ratios (ERs) of both SMZI and FMZI modulators are >25 dB. The propagation loss of the TFLN waveguide, extracted using a ring resonator, is about 0.15 dB/cm [15]. Therefore, <1 dB insertion loss of the devices should be anticipated. The relatively larger insertion loss measured here can be attributed to the write-field stitching errors in the long MZI arms from the electron beam lithography system (Raith Voyager). This problem can be avoided using, e.g., deep ultraviolet lithography technique for these centimeter-length structures. The half-wave voltages V_π was also measured for the SMZI and FMZI modulators

Optics EXPRESS

using a 100kHz triangular voltage sweep. The V_π values for the SMZI and FMZI modulators are 0.67 V and 0.70 V, respectively, corresponding to a $V_\pi L$ of ~2.2V·cm, which agrees well with the simulation results.

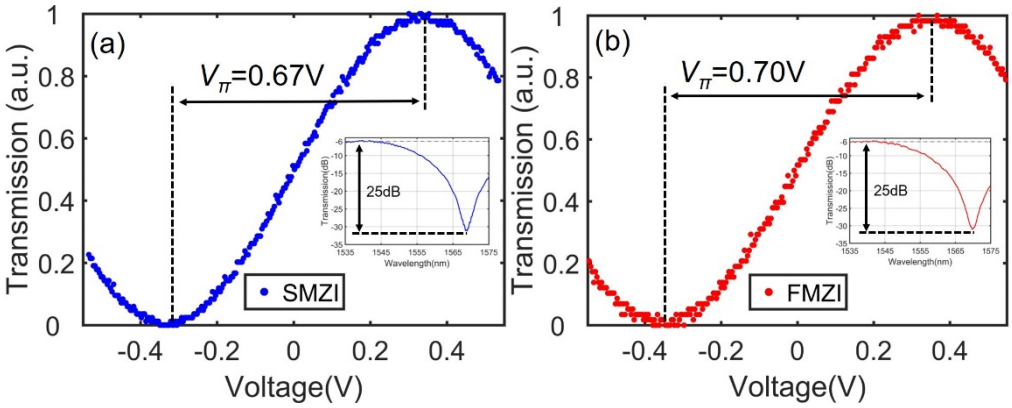

Fig. 3. Normalized optical transmissions as a function of the applied voltage for (a) SMZI modulator and (b) FMZI modulator. The V_π value for each device is also marked. The insets show the insertion losses and static ERs corresponding devices.

Next, we characterized the S parameters of the electrodes for the SMZI and FMZI modulators, and the RF effective index n_m and the RF loss α_m, which are key parameters for the bandwidth of a TW modulator, are also extracted as shown in Fig. 4. It is clearly seen that the RF effective indices n_m of both modulators nearly equal to the optical group index n_g, proving that the silicon undercut etching process was well controlled. From Fig. 4(d), the frequency independent characteristic RF losses α_0 of 0.33dBcm^{-1}GHz$^{-1/2}$ and 0.38dBcm^{-1}GHz$^{-1/2}$ can be deduced for the SMZI and FMZI modulators, respectively. As shown in Figs. 4(a), the measured S_{11} reflection is below −20 dB in the whole frequency span for the SMZI modulator, indicating that a good impedance matching has been achieved for the CLTW electrode. The measured S_{11} parameter of the FMZI modulator in Fig. 4(b), about −10 dB, is however higher. This larger reflection, as well as the large ripples in loss response, might come from the impedance discontinuity between the straight CLTW electrode and the U-turn with the normal TW electrode. This is also evident from the oscillations in the S_{11} frequency responses in Figs. 4(a) and 4(b). The residual oscillations in the S_{11} of the SMZI modulator may come from the impedance discontinuity between the electrode and the probes. The periods of the oscillations in S_{11} of the two cases show a difference of about three times, which matches the length difference of the straight sections of the electrodes. Although the higher RF reflection of the FMZI modulators would not largely affect the modulation performances as it will be shown below, it may still affect the single integrity of the driver electronics. Therefore, further optimizations in the transition structures between the straight and the bending electrodes of the FMZI modulator should be investigated. The small-signal EO responses were also further measured using a 70-GHz photodetector (PD, Finisar XPDV3120). The RF signal was applied to the fabricated devices using a high-speed RF probe, and another RF probe was used to provide a 50Ω termination. The EO responses of the SMZI and FMZI modulators are also shown in Figs. 4(a) and 4(b) with measured EO modulation bandwidths BW_{3dB} of 42 GHz and 45 GHz for the SMZI and FMZI modulators, respectively. The measured EO responses are matched well to the simulated EO responses using the measured electrode parameters. From the above analyses, one can find that the characteristics of the SMZI and FMZI modulators are close to each other, which indicates that the folded structure would not affect the modulation performances.

Optics EXPRESS

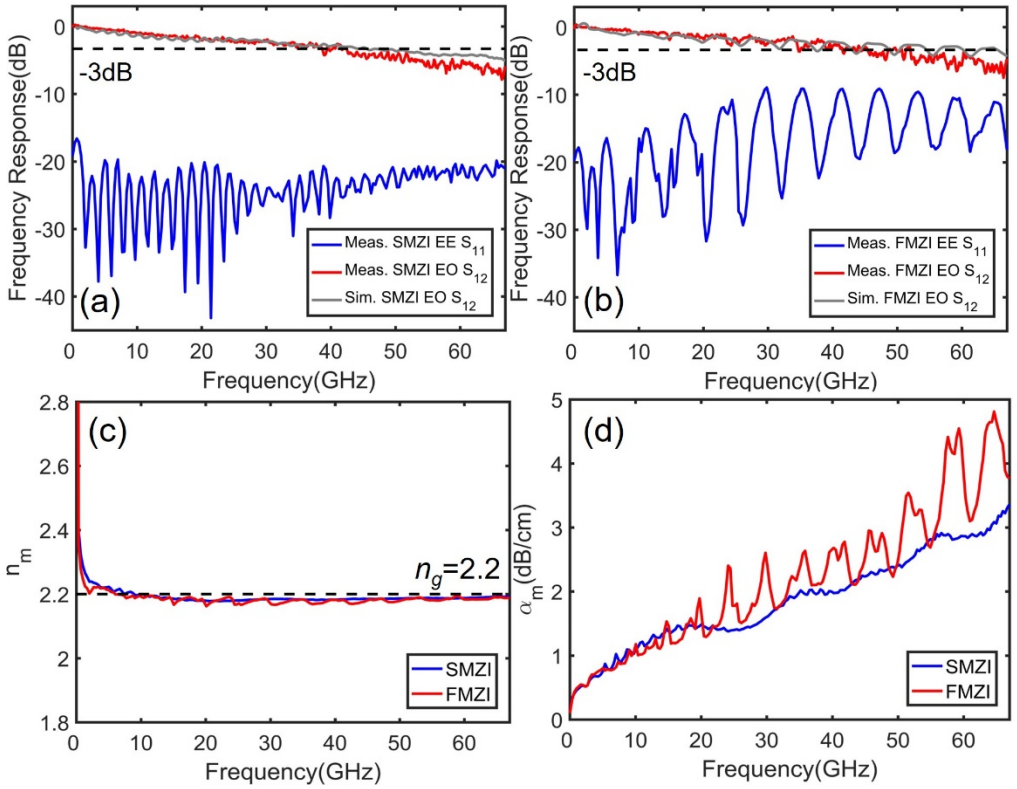

Fig. 4. Measured electrode S_{11} reflection, measured EO S_{12} response, and simulated EO S_{12} response of (a) SMZI modulator and (b) FMZI modulator using the corresponding measured electrode parameters. (c) Extracted RF effective indices n_m and (d) RF losses α_m of the SMZI and FMZI modulators. The black dashed line in (c) refers to the optical group index of $n_g = 2.2$.

Since the fabricated devices exhibits halfwave voltages V_π of about 0.7 V, it is possible to drive the modulators using direct outputs from CMOS circuits without any RF amplifiers. This can dramatically improve the system performances and reduce power consumption. In order to further verify this driverless operation of the fabricated modulators, high-speed data transmissions of the SMZI and FMZI modulators were also characterized, as shown in Fig. 5. The experimental setups for measuring the eye diagram and back-to-back (B2B) bit-error rates (BERs) are shown in Fig. 5(a). During the measurements, the data signal was generated by a 256GS/s arbitrary wave generator (AWG) with an analog bandwidth of 70 GHz (Keysight M8199A). The RF signal was fed directly to the device under test (DUT). A tunable laser source of about 0dBm output power was used as the light input, and the modulated light was amplified by an erbium-doped fiber amplifier (EDFA) and filtered by a bandpass filter (BPF). It was finally detected by the high-speed PD. Due to the high-power handling capability of the TFLN devices, using a high-power laser source as the input instead of an EDFA can minimize the additional noise and improve the system performance. The eye diagrams were recorded using a sampling oscilloscope (Agilent 86100D) with a bandwidth of 80 GHz.The eye diagrams for 100Gbaud OOK, 64Gbaud PAM-4, and 50Gbaud PAM-8 signals after the FMZI modulator are shown in Figs. 5(b)–5(d). The dynamic ERs reach 5.7 dB. Figures 6(a) and 6(b) show the B2B BERs of the 64Gbaud and 100Gbaud PAM-4 signal for the SMZI and FMZI modulators, respectively. Here, the received optical

Optics EXPRESS

power was measured just before the high-speed PD, and the detected signals were collected by a real-time oscilloscope (Labmaster 10 Zi-A) with a bandwidth of 59 GHz and a sampling rate of 160GS/s, and the BERs were calculated off-line using simple feed-forward equalizer (FFE) based linear digital signal process (DSP) algorithms. The BERs can drop below the KP-4 forward error correction (FEC) threshold (2.4×10^{-4}) for both cases. The insets of Fig. 6(b) demonstrate the calculated eye diagrams after DSP for the 100Gbaud PAM-4 signals at a received optical power of −9dBm for the SMZI and FMZI modulators. It is clearly seen that the performances of high-speed data transmissions for both modulators are very similar with no obvious power penalty between them. The modulation energy consumption of the fabricated FMZI modulator can be estimated as 4.49fj/bit for the 100Gbaud PAM-4 modulation format, which is one-tenth of that for a TFLN modulator based on the regular TW electrode [12]. To the best of our knowledge, this is the first demonstration to achieve beyond 100GBaud PAM-4 modulation (200Gb/s) within the KP-4 FEC threshold without using an RF amplifier on the TFLN platform. Although silicon or InP based modulators can also support this single-lane 100GBaud intensity modulation, the requirement of an RF amplifier largely increases the power consumption of transmitter modules using these modulators [22].

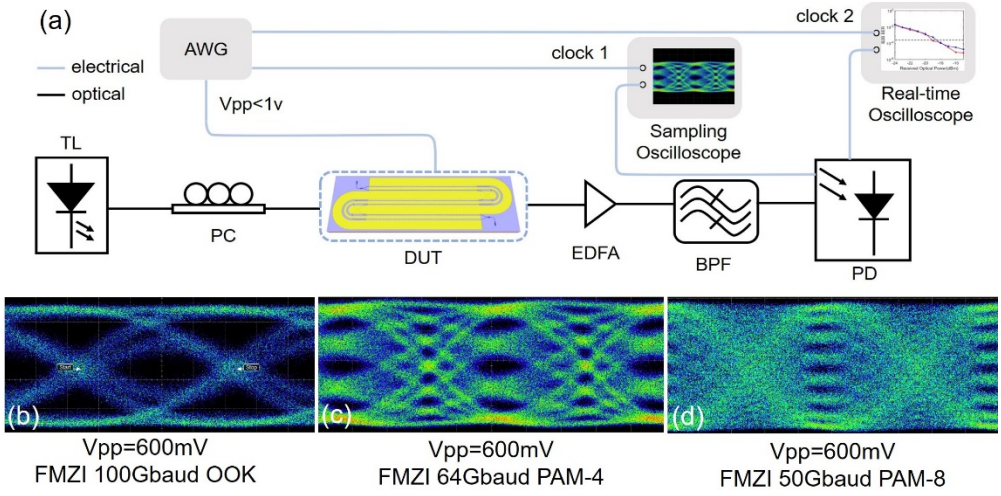

Fig. 5. (a) Experimental setups for measuring the eye diagram and B2B BERs. Measured optical eye diagrams for the FMZI modulator at data rates of (b) 100Gbaud OOK, (c) 64Gbaud PAM-4, and (d) 50Gbaud PAM-8.

Optics EXPRESS

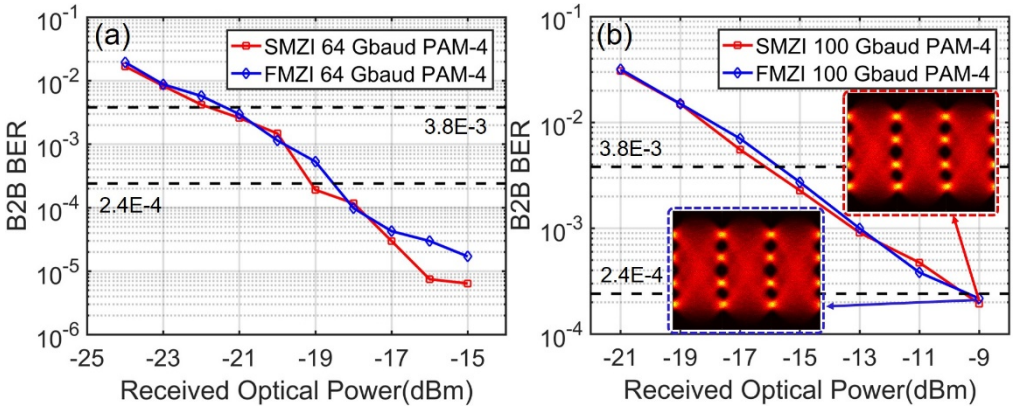

Fig. 6. Measured B2B BERs as a function of the received optical power for the SMZI and FMZI modulators of (a) 64Gbaud and (b) 100Gbaud PAM-4 signals. The insets in (b) show the calculated eye diagrams for 100Gbaud PAM-4 signals after DSP.

4. Conclusion

We have demonstrated an FMZI modulator using the CLTW electrode on a silicon substrate based on the TFLN platform. As shown in Fig. 7, The voltage-bandwidth performances of the fabricated devices reach 100 GHz/V^2, which are comparable with that of a similar TFLN modulator on a quartz substrate [13,14], and more preferable than other TFLN modulators on a silicon substrate using a regular TW electrode [12]. Moreover, the device length in the present design has been shortened through the folded structure without affecting the modulation performances. Obviously, it can be further compressed using more U-turns, and potentially be adapted to fit in a compact transceiver package, such as QSFP-DD (quad small form-factor pluggable double-density). The width of the present FMZI can also be reduced by optimizing the bending radius of the electrode. Even more intriguing is the feasibility to perform the 100GBaud PAM-4 modulation from a direct CMOS output without using any RF drivers. Combining the hybrid integration technology of a semiconductor laser [23], the demonstrated compact TFLN modulator structure could support a

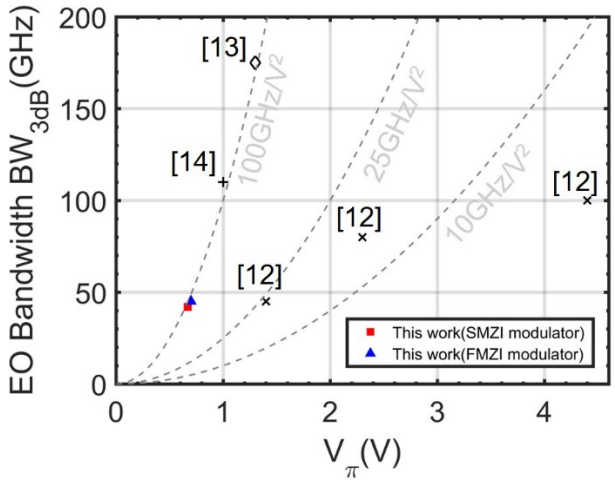

Fig. 7. Comparison of voltage-bandwidth performances of some TFLN modulators.

Optics EXPRESS

driverless single-lane 100Gbaud data transmission with an energy consumption of several fj/bit for next-generation transceiver interfaces operating at ultrahigh speed and low power. It is also possible to integrate the proposed device structure on a silicon photonic chip by using, e.g., the heterogeneous integration technology [17,24].

Funding. National Key Research and Development Program of China (2019YFB1803902); National Natural Science Foundation of China (62135012, 62105107, 91950205, 61961146003, 92150302); Leading Innovative and Entrepreneur Team Introduction Program of Zhejiang (2021R01001); Basic and Applied Basic Research Foundation of Guangdong Province (2021A1515012215, 2021B1515120057); Science and Technology Planning Project of Guangdong Province (2019A050510039); Fundamental Research Funds for the Central Universities (2021QNA5001).

Disclosures. The authors declare no conflicts of interest.

Data availability. Data underlying the results presented in this paper are not publicly available at this time but may be obtained from the authors upon reasonable request.

References

1. N. Jones, "How to stop data centres from gobbling up the world's electricity," Nature **561**(7722), 163–166 (2018).
2. D. A. B. Miller, "Energy consumption in optical modulators for interconnects," Opt. Express **20**(S2), A293–A308 (2012).
3. I. P. Kaminow, T. Li, and A. E. Willner, *Optical Fiber Telecommunications VB: Systems and Networks* (Elsevier Academic, 2013).
4. M. Li, W. Lei, X. Li, X. Xiao, and S. Yu, "Silicon intensity Mach-Zehnder modulator for single lane 100Gb/s applications," Photon. Res. **6**(2), 109–116 (2018).
5. S. Ummethala, J. N. Kemal, A. S. Alam, M. Lauermann, A. Kuzmin, Y. Kutuvantavida, S. H. Nandam, L. Hahn, D. L. Elder, L. R. Dalton, T. Zwick, S. Randel, W. Freude, and C. Koos, "Hybrid electro-optic modulator combining silicon photonic slot waveuides with high-k radio-frequency slotlines," Optica **8**(4), 511–519 (2021).
6. A. Melikyan, K. Koehnle, M. Lauermann, R. Palmer, S. Koeber, S. Muehlbrandt, P. C. Schindler, D. L. Elder, S. Wolf, W. Heni, C. Haffner, Y. Fedoryshyn, D. Hillerkuss, M. Sommer, L. R. Dalton, D. Van Thourhout, W. Freude, M. Kohl, J. Leuthold, and C. Koos, "Plasmonic-organic hybrid (POH) modulators for OOK and BPSK signaling at 40 Gbit/s," Opt. Express **23**(8), 9938–9946 (2015).
7. Y. Ogiso, J. Ozaki, Y. Ueda, H. Wakita, M. Nagatani, H. Yamazaki, M. Nakamura, T. Kobayashi, S. Kanazawa, Y. Hashizume, H. Tanobe, N. Nunoya, M. Ida, Y. Miyamoto, and M. Ishikawa, "80-GHz bandwidth and 1.5-V Vπ InP-based IQ modulator," J. Lightwave Technol. **38**(2), 249–255 (2020).
8. M. Sakib, P. Liao, C. Ma, R. Kumar, D. Huang, G. Su, X. Wu, S. Fathololoumi, and H. Rong, "A high-speed micro-ring modulator for next generation energy-efficient optical networks beyond 100 Gbaud," in *Conference on Lasers and Electro-Optics (CLEO), OSA Technical Digest* (Optical Society of America, 2021), paper SF1C.3.
9. S. Koeber, R. Palmer, M. Lauermann, W. Heni, D. L. Elder, D. Korn, M. Woessner, L. Alloatti, S. Koenig, P. C. Schindler, H. Yu, W. Bogaerts, L. R. Dalton, W. Freude, J. Leuthold, and C. Koos, "Femtojoule electro-optic modulation using a silicon-organic hybrid device," Light Sci. Appl. **4**(2), e255 (2015).
10. C. Kieninger, Y. Kutuvantavida, D. L. Elder, S. Wolf, H. Zwickel, M. Blaicher, J. N. Kemal, M. Lauermann, S. Randel, W. Freude, L. R. Dalton, and C. Koos, "Ultra-high electro-optic activity demonstrated in a silicon-organic hybrid (SOH) modulator," Optica **5**(6), 739–748 (2018).
11. C. Kieninger, Y. Kutuvantavida, H. Miura, J. N. Kemal, H. Zwickel, F. Qiu, M. Lauermann, W. Freude, S. Randel, S. Yokoyama, and C. Koos, "Demonstration of long-term thermally stable silicon-organic hybrid modulators at 85 °C," Opt. Express **26**(21), 27955–27964 (2018).
12. C. Wang, M. Zhang, X. Chen, M. Bertrand, A. Shams-Ansari, S. Chandrasekhar, P. Winzer, and M. Loncar, "Integrated lithium niobate electro-optic modulators operating at CMOS-compatible voltages," Nature **562**(7725), 101–104 (2018).
13. P. Kharel, C. Reimer, K. Luke, L. He, and M. Zhang, "Breaking voltage-bandwidth limits in integrated lithium niobate modulators using micro-structured electrodes," Optica **8**(3), 357–363 (2021).
14. M. Xu, Y. Zhu, F. Pittala, J. Tang, M. He, W. C. Ng, J. Wang, Z. Ruan, X. Tang, M. Kuschnerov, L. Liu, S. Yu, B. Zheng, and X. Cai, "Dual-polarization thin-film lithium niobate in-phase quadrature modulators for terabit-per-second transmission," Optica **9**(1), 61–62 (2022).
15. G. Chen, K. Chen, R. Gan, Z. Ruan, Z. Wang, P. Huang, C. Lu, A. P. T. Lau, D. Dai, C. Guo, and L. Liu, "High performance thin-film lithium niobate modulator on a silicon substrate using periodic capacitively loaded traveling-wave electrode," APL Photon. **7**(2), 026103 (2022).
16. J. Hu, C. Li, C. Guo, C. Lu, A. P. T. Lau, P. Chen, and L. Liu, "Folded thin-film lithium niobate modulator based on a poled Mach–Zehnder interferometer structure," Opt. Lett. **46**(12), 2940–2943 (2021).
17. S. Sun, M. Xu, M. He, S. Gao, X. Zhang, L. Zhou, L. Liu, S. Yu, and X. Cai, "Floded heterogeneous silicon and lithium niobate Mach-Zehnder modulators with low drive voltage," Micromachines **12**(7), 823 (2021).
18. X. Chen, S. Chandrasekhar, S. Randel, G. Raybon, A. Adamiecki, P. Pupalaikis, and P. J. Winzer, "All-electronic 100-GHz bandwidth digitalto-analog converter generating PAM signals up to 190 GBaud," J. Lightwave Technol. **35**(3), 411–417 (2017).

Optics EXPRESS

19. Z. Ruan, J. Hu, Y. Xue, J. Liu, B. Chen, J. Wang, K. Chen, P. Chen, and L. Liu, "Metal based grating coupler on a thin-film lithium niobate waveguide," Opt. Express **28**(24), 35615–35621 (2020).
20. B. Chen, Z. Ruan, J. Hu, J. Wang, C. Lu, A. P. T. Lau, C. Guo, K. Chen, P. Chen, and L. Liu, "Two-dimensional grating coupler on an X-cut lithium niobate thin-film," Opt. Express **29**(2), 1289–1295 (2021).
21. J. Cai, C. Guo, C. Lu, A. P. T. Lau, P. Chen, and L. Liu, "Design Optimization of Silicon and Lithium Niobate Hybrid Integrated Traveling-wave Mach-Zehnder Modulator," IEEE Photon. J. **13**, 2200206 (2021).
22. M. Jacques, Z. Xing, A. Samani, X. Li, E. El-Fiky, S. Alam, O. Carpentier, P. Koh, and D. V. Plant, "Net 212.5 Gbit/s Transmission in O-band With a SiP MZM, One Driver and Linear Equalization," in *Optical Fiber Communication Conference Post deadline Papers 2020*, (Optica Publishing Group, 2020), paper Th4A.3.
23. A. Shams-Ansari, D. Renaud, R. Cheng, L. Shao, L. He, D. Zhu, M. Yu, H. R. Grant, L. Johansson, M. Zhang, and M. Lončar, "Electrically pumped laser transmitter integrated on thin-film lithium niobate," Optica **9**(4), 408–411 (2022).
24. M. He, M. Xu, Y. Ren, J. Jian, Z. Ruan, Y. Xu, S. Gao, S. Sun, X. Wen, L. Zhou, L. Liu, C. Guo, H. Chen, S. Yu, L. Liu, and X. Cai, "High-performance hybrid silicon and lithium niobate Mach-Zehnder modulators for 100 Gbit s-1 and beyond," Nat. Photonics **13**(5), 359–364 (2019).